AIP | Review of Scientific Instruments

Calibration and sensitivity of the infrared imaging video bolometer

B. J. Peterson, A. Yu. Kostrioukov, N. Ashikawa, M. Osakabe, and S. Sudo

Citation: Rev. Sci. Instrum. **74**, 2040 (2003); doi: 10.1063/1.1537031
View online: http://dx.doi.org/10.1063/1.1537031
View Table of Contents: http://rsi.aip.org/resource/1/RSINAK/v74/i3
Published by the American Institute of Physics.

Calibration and sensitivity of the infrared imaging video bolometer

B. J. Peterson,[a] A. Yu. Kostrioukov, N. Ashikawa, M. Osakabe, and S. Sudo
National Institute for Fusion Science, Toki-shi 509-5292, Japan

(Presented on 10 July 2002)

The infrared (IR) imaging video bolometer (IRVB) is an imaging bolometer which uses a large (9 cm×9 cm) thin (1 μm) gold foil and an IR camera to provide images of radiation from the plasma. Calibration of the IRVB using a lamp has been performed to compensate for any nonuniformities in the foil's thickness and its thermal properties due to blackening of the foil with graphite to improve the IR emissivity. This calibration revealed close to expected values for the calibration coefficient proportional to the product of the thermal conductivity and the foil thickness in the central region of the foil, while these values were anomalously high near the foil edge. The calibration coefficient proportional to the thermal diffusivity is a factor of 2 smaller than the expected value at the center and drops further at the edge of the foil. Using a derived expression for the IRVB noise equivalent power, a sensitivity comparison shows the IRVB using current IR technologies to be ~200 times less sensitive than an equivalent conventional resistive bolometer operating under ideal conditions.
[DOI: 10.1063/1.1537031]

I. INTRODUCTION

Bolometers are important diagnostics for measuring the local and global radiated power from magnetically confined plasmas.[1,2] Bolometric measurements have primarily utilized resistive metal foil detectors.[3,4] In recent years, infrared (IR) technology has been applied to the development of imaging bolometers.[5–12] This has lead to a concept known as the infrared imaging video bolometer (IRVB)[9] based on a large free-standing thin metal foil, the front side of which absorbs the incident radiation from the plasma through a pinhole. The resulting change in the temperature of the foil is measured by an IR camera viewing the graphite blackened, back side of the foil from outside the vacuum vessel through an IR vacuum window. The foil is divided up numerically into bolometer pixels consisting of one or more IR camera pixels and the heat diffusion equation is solved for the radiated power on the foil considering the losses due to the blackbody radiation from the blackened back side of the foil.[12]

To date, this diagnostic has demonstrated the ability to provide qualitative images of the plasma radiation.[10–12] However, in order to fully utilize this diagnostic for physics studies requiring quantitative tomographic analyses of radiation from divertor and core regions, a calibration technique is necessary which gives an adequate level of confidence in the absolute and relative levels of the measured values. In this article, we address this issue by describing the experimental setup in Sec. II and three different calibration experiments and their results in Sec. III. In Sec. IV an expression is provided for the sensitivity of the diagnostic based on an improved numerical algorithm for solving the heat diffusion equation including the blackbody radiation losses of the foil. This expression is then used to make a comparison of the sensitivity of the IRVB with an equivalent resistive bolometer. Finally, a discussion of the results is given in Sec. V with some suggestions for improving the calibration and the sensitivity of the IRVB.

II. SETUP FOR CALIBRATION EXPERIMENTS

The foil and frame are shown in Fig. 1 and are similar to that described previously.[9] The gold foil is 10 cm×10 cm ×1 μm thick sandwiched between two 2 mm thick, 13.5 cm diameter copper frames with a 9 cm×9 cm hole in each frame which exposes the foil on either side. Sixteen bolts are used to clamp the frames together insuring good thermal contact between the frame and foil. The IR camera side of the foil is blackened with graphite, while the side exposed to the radiation source (or plasma in actual use) is left as bare gold. The outer sides of the frames are similarly blackened prior to assembly. The framed foil is mounted in a vacuum chamber which is then evacuated to less than 1 mTorr to avoid cooling of the foil by collisions with room-temperature molecules and neutral particles.

The foil is mounted in the vacuum chamber approximately 4.5 cm behind a vacuum window with an inner diameter of 14 cm. A 500 W lamp with a 16 cm diam parabolic reflector is mounted 20 cm in front of the window. On the other side of the vacuum chamber a ZnSe IR window coated for a flat transmission response of >95% over the range 3–12 μm is mounted on a flange. The blackened side of the foil is then viewed through this window with an AGEMA LW900 IR camera (15 Hz, 272×136 pixels, 8–12 μm). The view of the exposed foil encompasses 136 (horizontal) ×131 (vertical) IR camera pixels.

III. CALIBRATION OF IRVB

The temperature on the foil, $T(x,y,t)$, at the position (x,y) (horizontal, vertical), and at time t is determined by the two-dimensional heat diffusion equations,

[a]Electronic mail: peterson@LHD.nifs.ac.jp

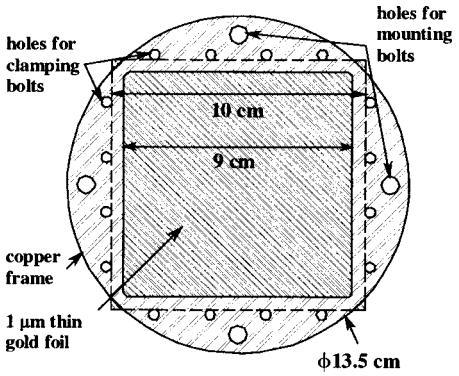

FIG. 1. Drawing of frame and mask for calibration experiments.

$$\Omega_L = \frac{\Omega_t}{C_2} - \frac{\Omega_{\rm rad}}{C_3} + \frac{\Omega_{\rm bb}}{C_1}, \tag{1}$$

$$\Omega_L = \frac{\partial^2 T}{\partial x^2} + \frac{\partial^2 T}{\partial y^2}, \tag{2}$$

$$\Omega_t = \frac{1}{\kappa}\frac{\partial T}{\partial t}, \tag{3}$$

$$\Omega_{\rm rad} = \frac{S_{\rm rad}}{k t_f}, \tag{4}$$

$$\Omega_{\rm bb} = \frac{\varepsilon \sigma_{\rm S\text{-}B}(T^4 - T_0^4)}{k t_f}, \tag{5}$$

where Ω_L is the two-dimensional Laplacian term, Ω_t is the time derivative term, $\Omega_{\rm rad}$ is the radiation source term, and $\Omega_{\rm bb}$ is the blackbody radiation loss term given by the Stefan-Boltzmann equation. The other parameters are given as the thermal diffusivity of gold, $\kappa = 1.27\ {\rm cm}^2/{\rm s}$, the thermal conductivity of gold, $k = 3.16\ {\rm W/cm\,K}$, the incident radiated power density, $S_{\rm rad}$, the thickness of the foil, t_f, the blackbody emissivity of the foil, $\varepsilon \sim 1$, the Stefan-Boltzmann constant, $\sigma_{\rm S\text{-}B} = 5.67 \times 10^{-12}\ {\rm W/cm^2\,K^4}$, the temperature of the background structure (room temperature), T_0, and calibration coefficients, C_1, C_2, C_3. Ideally the calibration coefficients should each be equal to one, but in the cases of nonuniformities in the foil thickness or variation of the thermal properties of the foil due to the graphite blackening, the calibration coefficients should be determined for each part of the foil. In order to determine these coefficients and check the accuracy of the calculation of $S_{\rm rad}$, three calibration experiments were devised.

A. First calibration experiment

In this experiment, the frame and foil are heated by the lamp up to a temperature of about 20 °C above room temperature, and then the lamp is turned off. The temperature of the relatively massive frame cools very slowly while the foil is cooled rapidly by the blackbody radiation. The foil quickly reaches a steady state wherein the edge of the foil is at frame temperature and the center of the foil is at room temperature as can be seen in Fig. 2(a). In this case, the heat diffusion equation is reduced to two terms, the Laplacian and the blackbody radiation terms. The calibration coefficient is then given by $C_1 = \Omega_{\rm bb}/\Omega_L$. Data for this experiment was taken for 10 s and the resulting 150 frames were averaged together to remove the noise from temporal temperature fluctuations. The profile is shown in Fig. 1(a). The foil temperature is then resampled to 13×13 points using a linear interpolation resampling routine [CONGRID (Ref. 13)]. Then the two-dimensional temperature profile is fit to a sixth-order polynomial in two dimensions [SFIT (Ref. 13)]. The three different temperature profiles across the horizontal mid-plane of the foil are shown in Fig. 2(a). Using the polynomial fitting parameters the Laplacian is calculated analytically and the blackbody radiation term is computed directly as are shown in Fig. 2(b). Then using these values C_1 is calculated from their ratio as described above. At the center the ratio is poorly defined as both values approach zero, therefore these anomalous values have been arbitrarily set to 1.

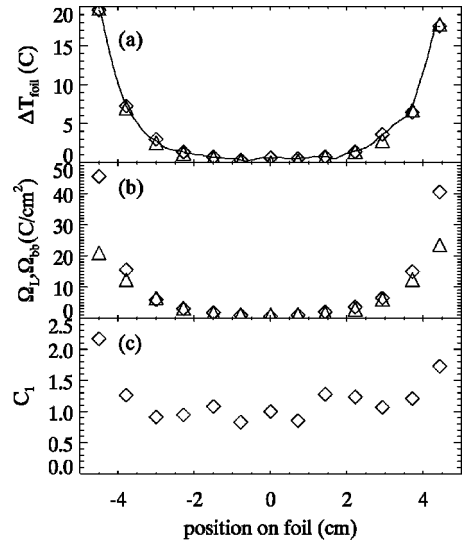

FIG. 2. Profiles at the horizontal midplane of the foil for (a) ΔT—raw data (line), resampled data (diamond), fitted data (triangle), (b) $\Omega_{\rm bb}$ (diamond), Ω_L (triangle), and (c) C_1.

One notes that the fitted data are slightly lower than the resampled and raw temperature data. The blackbody term is much higher than the Laplacian at the edges which results in the anomalously high values of C_1 at the edge. The other values are close to the expected value of one (ignoring the three inner points, which result from the indeterminate ratio of two numbers close to zero).

B. Second calibration experiment

In the next experiment, the foil was quickly heated (within 1 s) with the lamp up to thermal equilibrium without heating the frame and then the lamp was turned off and the decaying foil temperature was measured. This results in the heat diffusion equation being reduced to three terms, excluding the radiation source term. Then C_2 can be solved for from $C_2 = \Omega_t/(\Omega_L - \Omega_{\rm bb}/C_1)$. The data were analyzed by first resampling the raw data to a 13×13 grid with CONGRID and then using a gradient expansion algorithm to compute a nonlinear least-squares fit [CURVEFIT (Ref. 13)] of each of the grid point's time histories to an exponential decay. The three-dimensional array is then resampled in time

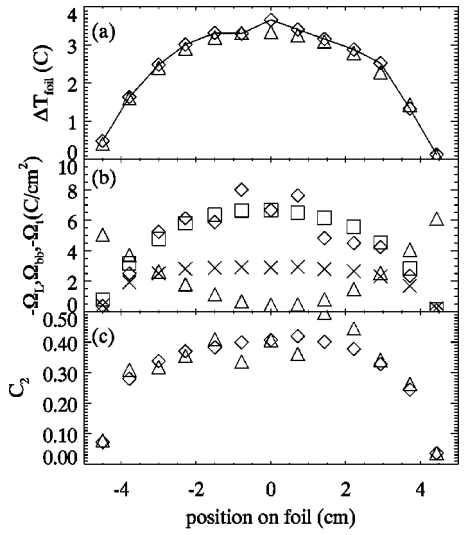

FIG. 3. Profiles at the horizontal midplane of the foil for (a) ΔT—exponentially fitted (line), resampled (diamond), surface fitted (triangle), (b) corrected Ω_{bb} (diamond), Ω_{bb} (square), $-\Omega_L$ (triangle), $-\Omega_t(x)$, and (c) C_2 (diamond), corrected C_2 (triangle).

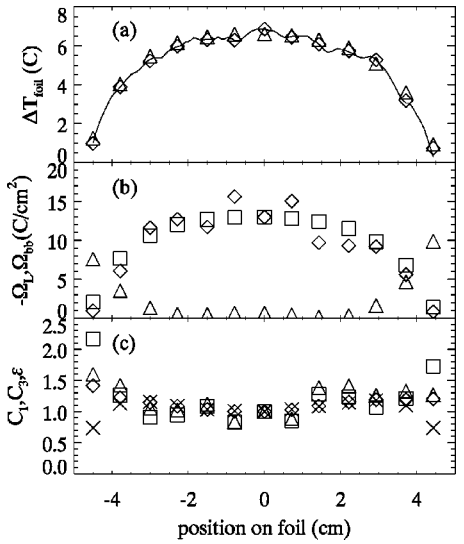

FIG. 4. Profiles at the horizontal midplane of the foil for (a) ΔT—raw data (line), resampled data (diamond), fitted data (triangle), (b) corrected Ω_{bb} (diamond), Ω_{bb} (square), $-\Omega_L$ (triangle), and (c) C_3 (diamond), corrected C_3 (triangle), C_1 (square), $\varepsilon(x)$.

and the timing equivalent to 670 ms after the beginning of the decay is selected for the analysis. This two-dimensional array is then fit to a fifth-order polynomial in two dimensions (SFIT). These temperature profiles are show in Fig. 3(a). The surface fit is used to calculate Ω_L and Ω_{bb} while the exponential fitting parameters are used to calculate Ω_t. These terms are shown in Fig. 3(b) with Ω_{bb} also shown corrected by C_1. Then C_2 is calculated according to the expression given above with and without the correction of C_1 and both profiles are plotted in Fig. 3(c).

In this data set also the fitted temperatures are slightly lower than the original values. Ω_L has the opposite sign of the previous case due to the change in the direction of the heat diffusion. Ω_t has a rather flat profile, dropping suddenly at the edges as does C_2. Even the peak vales of C_2 are half of what is expected.

C. Third calibration experiment

In this experiment, the foil was quickly heated (within 1 s) by the lamp to a thermal equilibrium condition without heating the frame and 10 s of data were taken. In this case, a 1 mm thick sheet of teflon was placed between the foil and the lamp at the position of the window to provide a uniform (to within 1%) light source. This experiment eliminates the time derivative term of the heat diffusion equation and allows one to solve for C_3 using $C_3=\Omega_{rad}/(\Omega_{bb}/C_1-\Omega_L)$. The data was analyzed in the same manner as in the first experiment with and with out the correction of C_1. C_3 is normalized to the center pixel, as the absolute value of S_{rad} from the lamp is not known. The effective blackbody emissivity of the foil ε can be calculated from $\varepsilon=C_3/C_1$ (C_3 calculated using C_1).

The wavelike structure seen in the raw temperature profile may be from uncompensated reflections on wrinkles in the foil. These are removed through the fitting. C_3 is much more uniform over the foil than C_1. This is seen to be due to the better balance between $-\Omega_L$ and Ω_{bb} in Fig. 4(b). The ε value is also fairly constant and close to the expected value of one except at the edges.

IV. SENSITIVITY OF IRVB

Previously, an expression for the numerical solution of Eq. (1) for S_{rad} was given using an explicit differencing scheme.[9] We improve on this method by using a Crank-Nicholson scheme[14] and also include the blackbody radiation term given in Eq. (5) to give

$$S_{rad}=kt_f[\Omega_t-\Omega_L+\Omega_{bb}], \tag{6}$$

where

$$\Omega_t=\frac{1}{\kappa\Delta t}\left[T\left(x,y,t+\frac{\Delta t}{2}\right)-T\left(x,y,t-\frac{\Delta t}{2}\right)\right], \tag{7}$$

$$\Omega_{bb}=\frac{\varepsilon\sigma_{S\text{-}B}}{2kt_f}\left[\begin{array}{c}T^4\left(x,y,t+\frac{\Delta t}{2}\right)+T^4\left(x,y,t-\frac{\Delta t}{2}\right)\\ -T_0^4\left(t+\frac{\Delta t}{2}\right)-T_0^4\left(t-\frac{\Delta t}{2}\right)\end{array}\right], \tag{8}$$

$$-\Omega_L=\frac{1}{2l^2}\left\{\begin{array}{l}\left[\begin{array}{c}4T(x,y)-T(x,y+l)-T(x,y-l)\\ -T(x+l,y)-T(x-l,y)\end{array}\right]_{t+\Delta t/2}\\ +\left[\begin{array}{c}4T(x,y)-T(x,y+l)-T(x,y-l)\\ -T(x+l,y)-T(x-l,y)\end{array}\right]_{t-\Delta t/2}\end{array}\right\} \tag{9}$$

and l is the spacing between bolometer pixels, t is time and Δt is the time resolution of the diagnostic, and x and y are the horizontal and vertical coordinates on the foil, respectively. Applying standard error analysis gives the following expression for the noise equivalent power:

$$\eta_{\mathrm{IRVB}}=\frac{\sqrt{10}kt_f\sigma_{\mathrm{IR}}}{\sqrt{mN}}\sqrt{1+\frac{l^4}{5\kappa^2m^2\Delta t_{\mathrm{IR}}^2}+\frac{4l^4\varepsilon^2\sigma_{\mathrm{S\text{-}B}}^2T^6}{5k^2t_f^2}} \tag{10}$$

in terms of the error in the IR camera measurement σ_{IR}, the time resolution of the IR camera, Δt_{IR}, and the number of frames averaged over m ($\Delta t=m\Delta t_{\mathrm{IR}}$), and the number of IR pixels per bolometer pixel N. The third term under the radical due to the blackbody radiation has a negligible contribution to the error near room temperature. If we compare this to a resistive metal foil bolometer with the same foil thickness $t_f=4\ \mu$m, material (gold), detector area $l^2=0.06\ \mathrm{cm}^2$ and $\Delta t=0.01$ s for a state-of-the-art IR camera with the following parameters $\sigma_{\mathrm{IR}}=0.02$ K, $\Delta t_{\mathrm{IR}}=2.38$ ms, 320×240 pixels then we get a noise equivalent power density of $190\ \mu\mathrm{W/cm}^2$, which compares with $1\ \mu\mathrm{W/cm}^2$, for the resistive bolometer.[4]

V. DISCUSSION

Large values of C_1 at the edge are most likely due to an underestimation of the Laplacian in the region of sharp temperature gradients at the edge of the foil in the first experiment. This would also help to explain anomalously low values of calculated power at the edge of the foil seen in experimental results form the IRVB mounted on the upper port in the large helical device. There might be two possible solutions to this problem. One would be to develop a better fitting routine than the sixth-order polynomial used in the analysis. Another possible solution would be to reduce the temperature gradient at the edge of the foil by insulating the foil from the frame and thereby dropping some of the temperature difference between the frame and the center of the foil in the insulation layer. This would essentially reduce the Laplacian diffusive term in Eq. (1) and raise the overall temperature of the foil and thereby increase the blackbody radiation term which is essentially the signal measured by the IR camera. This increase in signal due to the insulation should result in a more sensitive diagnostic and one easier to calibrate. Another method to calibrate the foil would be to use a laser of a known power distribution to make a local absolute calibration. Due to the small spot size and low power of the laser, we have not been able to do this for lack of a closeup lens for the IR camera. However, we will acquire such a lens in the near future and plan to carry out such calibration experiments at that time. Until these problems are resolved we can neglect the edge pixels after the analysis. It should also be mentioned that for a fusion reactor the thickness of the foils would need to be increased (in excess of 10 μm) in order to stop the expected higher-energy photons. In such a case, the concerns about the effects of blackening and nonuniformities in the foil thickness on calibration would be greatly diminished.

Comparison of sensitivity of the IRVB using a state-of-the-art IR camera with an equivalent metal foil resistive bolometer in terms of time response, detector size, and foil parameters shows that the IRVB is ~200 times less sensitive. However, these are for optimal conditions. Since the resistive bolometers are much more susceptible to electromagnetic noise, the IRVB should be competitive with the resistive bolometers in terms of sensitivity in an experimental environment, especially as the sensitivity of IR cameras continues to improve and their pixel number and speed increases. Also for the equivalent space taken by the resistive bolometer head, an imaging bolometer could provide 20 times the number of channels in two dimensions at a much lower cost with no vacuum feedthroughs.

ACKNOWLEDGMENTS

The authors would like to thank Professor K. Itoh of NIFS and Professor H. Zushi of Kyushu University for discussions regarding the differencing schemes used to solve the heat diffusion equation. The authors appreciate the support and encouragement of Professor M. Fujiwara and Professor O. Motojima of NIFS.

[1] H. Hsuan, K. Bol, and R. A. Ellis, Nucl. Fusion **15**, 657 (1975).
[2] A. W. Leonard, W. H. Meyer, B. Geer, D. M. Behne, and D. N. Hill, Rev. Sci. Instrum. **66**, 1201 (1995).
[3] G. Miller, J. C. Ingraham, and L. S. Schrank, Rev. Sci. Instrum. **53**, 1410 (1982).
[4] K. F. Mast, J. C. Vallet, C. Andelfinger, P. Betzler, H. Kraus, and G. Schramm, Rev. Sci. Instrum. **62**, 744 (1991).
[5] G. A. Wurden, in *Diagnostics for Experimental Thermonuclear Fusion Reactors*, edited by P. E. Stott *et al.* (Plenum, New York, 1996), pp. 603–606.
[6] G. A. Wurden, B. J. Peterson, and S. Sudo, Rev. Sci. Instrum. **68**, 766 (1997).
[7] G. A. Wurden and B. J. Peterson, Rev. Sci. Instrum. **70**, 255 (1999).
[8] N. Ashikawa, B. J. Peterson, G. A. Wurden, and S. Sudo, J. Plasma Fusion Res. **3**, 436 (2000).
[9] B. J. Peterson, Rev. Sci. Instrum. **71**, 3696 (2000).
[10] B. J. Peterson, N. Ashikawa, M. Osakabe, and M. Shoji, Rev. Sci. Instrum. **72**, 923 (2001).
[11] N. Ashikawa, B. J. Peterson *et al.*, J. Plasma Fusion Res. **4**, 437 (2001).
[12] B. J. Peterson, N. Ashikawa, A. Yu. Kostrioukov, K. Nishimura, H. Kojima, and S. Sudo, IEEE Trans. Plasma Sci. **30**, 52 (2002).
[13] From IDL, Research Systems Incorporated, www.rsi.com.
[14] W. H. Press *et al.*, *Numerical Recipes, the Art of Scientific Computing*, (Cambridge University Press, Cambridge, England 1986), pp. 635–642.